JCTC Journal of Chemical Theory and Computation

Article

pubs.acs.org/JCTC

Chemical Potentials, Activity Coefficients, and Solubility in Aqueous NaCl Solutions: Prediction by Polarizable Force Fields

Filip Moučka,[†] Ivo Nezbeda,[†,‡] and William R. Smith*[,¶,§]

[†]Faculty of Science, J. E. Purkinje University, 400 96 Ústí nad Labem, Czech Republic

[‡]Institute of Chemical Process Fundamentals, Academy of Sciences, 165 02 Prague 6, Czech Republic

[¶]Department of Mathematics and Statistics, University of Guelph, Guelph, Ontario N1G 2W1, Canada

[§]Faculty of Science, University of Ontario Institute of Technology, Oshawa, Ontario L1H 7K4, Canada

ABSTRACT: We describe a computationally efficient molecular simulation methodology for calculating the concentration dependence of the chemical potentials of both solute and solvent in aqueous electrolyte solutions, based on simulations of the salt chemical potential alone. We use our approach to study the predictions for aqueous NaCl solutions at ambient conditions of these properties by the recently developed polarizable force fields (FFs) AH/BK3 of Kiss and Baranyai (*J. Chem. Phys.* **2013**, *138*, 204507) and AH/SWM4-DP of Lamoureux and Roux (*J. Phys. Chem. B* **2006**, *110*, 3308−3322) and by the nonpolarizable JC FF of Joung and Cheatham tailored to SPC/E water (*J. Phys. Chem. B* **2008**, *112*, 9020−9041). We also consider their predictions of the concentration dependence of the electrolyte activity coefficient, the crystalline solid chemical potential, the electrolyte solubility, and the solution specific volume. We first highlight the disagreement in the literature concerning calculations of solubility by means of molecular simulation in the case of the JC FF and provide strong evidence of the correctness of our methodology based on recent independently obtained results for this important test case. We then compare the predictions of the three FFs with each other and with experiment and draw conclusions concerning their relative merits, with particular emphasis on the salt chemical potential and activity coefficient vs concentration curves and their derivatives. The latter curves have only previously been available from Kirkwood−Buff integrals, which require approximate numerical integrations over system pair correlation functions at each concentration. Unlike the case of the other FFs, the AH/BK3 curves are nearly parallel to the corresponding experimental curves at moderate and higher concentrations. This leads to an excellent prediction of the water chemical potential via the Gibbs−Duhem equation and enables the activity coefficient curve to be brought into excellent agreement with experiment by incorporating an appropriate value of the standard state chemical potential in the Henry Law convention.

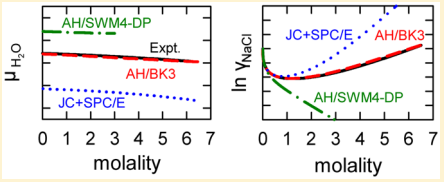

INTRODUCTION

Aqueous electrolyte solutions are ubiquitous in environmental, geochemical, metallurgical, and biological systems, and the ability to understand and predict their properties is of considerable interest and importance in many scientific communities. Advances in computational technology have facilitated the ability of molecular simulation methodologies using an empirical molecular interaction model whose parameters fitted to experimental or high-level ab initio computational data (a force field, FF), to provide both quantitative property predictions and microscopic insight for many fluid systems, including those involving aqueous solutions.[1−7]

Among the most important aqueous electrolyte solution properties are the solute and solvent chemical potentials over the entire experimentally accessible concentration range, and their accurate prediction is an important task. For example, in conjunction with the solid chemical potential, the electrolyte values determine the solubility. They also regulate the equilibrium concentrations of chemical reactions in solution, and their values in bulk solution govern the equilibrium behavior in molecularly confined environments (e.g., electrolytes in slits or pores). The chemical potentials of the water solvent are also important, since they determine the solvent vapor pressure lowering and the osmotic pressure for salt solutions.

An important application of the FF simulation approach is its extensive use in biomolecular simulations.[7] Since proteins and nucleic acids are surrounded by an aqueous electrolyte environment, the accuracy of the electrolyte FF can significantly affect the simulation results. Since most electrolyte FFs have been developed on the basis of low concentration data, including ion hydration free energy data at infinite dilution,[4,8−10] their use at higher concentrations is thereby questionable. It has often been noted[2,4,9−16] that biomolecular simulations using certain commonly available electrolyte FFs have exhibited electrolyte precipitation well below the experimental solubility limit, casting doubts on the suitability of such simulations at biologically relevant electrolyte concentrations.

In spite of its importance, only a small number of chemical potential related studies has been performed, very few of which have included solubility calculations. Most have involved

Received: January 8, 2015
Published: March 19, 2015

DOI: 10.1021/acs.jctc.5b00018
J. Chem. Theory Comput. 2015, 11, 1756−1764

relatively simple nonpolarizable FFs for NaCl solutions at ambient conditions,[17−29] which has become a benchmark test system for simulation methodologies and FFs.

Methodologies for chemical potential calculations in the literature have included different types of thermodynamic integration procedures within either a Monte Carlo (MC)[18,24] or Molecular Dynamics (MD)[19,22] setting, a Wang−Landau transition-matrix MC method,[20,21] and the Osmotic Ensemble MC (OEMC) method.[17,23,25−28,30] Solubility has been calculated by determining the intersection of the salt chemical potential vs concentration curve with the value of its crystal,[18−21,24] by direct calculation (in a single simulation) using a slab configuration MD method,[19,24,29] and by direct calculation using the OEMC method.[17,23,25,27,28]

Solubility results from different research groups for two simple nonpolarizable NaCl FFs compatible with the SPC/E water FF[31] are summarized in Table 1. As can be seen, they

Table 1. NaCl Solubility Calculations at T = 298.15 K and P = 1 bar Using SPC/E H_2O[31]

source	ion FF	method	molality
Joung and Cheatham, 2009[19]	JC[9]	MD with slab geometry	7.27(7)
Aragones et al., 2012[24]	JC[9]	MC and thermodynamic integration	4.8(3)
Aragones et al., 2012[24]	JC[9]	MD with slab geometry	5.5(4)
Aragones et al., 2012[24]	SD[50]	MC, thermodynamic integration	0.9(4)
Aragones et al., 2012[24]	SD[50]	MD with slab geometry	1.9(4)
Moučka et al., 2013[27]	JC[9]	OEMC	3.64(20)
Moučka et al., 2013[27]	SD[50]	OEMC	0.61
Kobayashi et al., 2014[29]	JC[9]	MD with slab geometry	6.20
Kobayashi et al., 2014[29]	JC[9]	MD and thermodynamic integration	6.42
Mester and Panagiotopoulos, 2014[32]	JC[9]	MD and particle insertion	3.59(4)
Mester and Panagiotopoulos, 2014[32]	SD[50]	MD and particle insertion	0.61(1)

exhibit significant disagreement. This is due to the facts that the solution chemical potential vs concentration curve tends to exhibit a reduced concentration dependence near the solubility limit[27] and that the simulated chemical potentials for aqueous electrolyte solutions are very sensitive to the details of the simulation procedure employed. With the disagreements of the research groups in mind and to explore our calculation procedure more deeply, in a recent study[26] we independently calculated both water and salt chemical potentials and verified their mutual consistency with respect to the Gibbs−Duhem equation. To our knowledge, this was the first such use of this procedure in conjunction with simulations, and it provided support for the correctness of our calculation procedures. This is further supported by the agreement of our results shown in Table 1 with the indicated recent calculations of Mester and Panagiotopoulos,[32] who used a different simulation methodology. We thus believe that the computational procedures used in the current study are sound and that the results of this paper are reliable.

Recently, we have shown[27] that a large class of widely used simple nonpolarizable FFs, consisting of charged Lennard-Jones spheres for the ions in combination with Lorentz−Berthelot combining rules and several of the commonly used water FFs, is inadequate for the accurate prediction of both aqueous solution chemical potentials and electrolyte solubility for aqueous NaCl solutions. Moreover, in a subsequent study,[28] we showed that attempts to improve such simple FFs by modifying their parameters is unlikely to be successful. It is becoming increasingly recognized that FFs based on the assumption of pairwise additivity are inadequate, both for pure water and its solutions, and that many-body effects must be incorporated. One possibility in this direction is to add polarizability to the interaction model, which mimics some of the effects of multibody molecular interactions. Many such FFs have been developed for pure H_2O, with varying degrees of success (see, for example, the review of Guillot[33]). Two recent promising proposals of this type have been suggested for H_2O by Lamoureux and Roux (SWM4-DP)[34] and by Kiss and Baranyai (BK3),[35] and aqueous alkali halide solution FFs have been tailored to them (AH/SWM4-DP[36] and AH/BK3,[37] respectively). The first of these mimics polarizability using a point-charge-on-spring (Drude) model, and the second uses a Gaussian-charge-on-spring distribution model.

Due to the increased complexity of polarizable FFs over their nonpolarizable counterparts, calculations of all properties are much more time-consuming and technically complicated than for the nonpolarizable case; this is particularly true for chemical potentials. Although simulations based on MD methods are parallelizable, this is not the case for MC methods, which are intrinsically serial in nature. To overcome this apparent disadvantage of MC methodology, we recently developed the Multi-Particle-Move Monte Carlo (MPM−MC) method,[30,38,39] which generates configurations by moving all particles simultaneously, similarly to the corresponding MD methodology and with which it hence shares the ability to be parallelized. The method has been found to be competitive with MD methods for polarizable force fields, although it realizes no computational efficiencies in the case of pairwise additive FFs. Since the OEMC algorithm is an open ensemble MC method, implementation in an MD algorithm is problematic. However, it is relatively easy to adapt it to the case of polarizable FFs in conjunction with the use of the MPM−MC method for generating configurations.

The primary goal of this paper is to propose and demonstrate a computationally efficient methodology for calculating the solution chemical potentials and activity coefficients of both solute and solvent, which is based on chemical potential simulations of the salt alone. We demonstrate our approach by showing new predictions for aqueous NaCl solutions at ambient conditions (T = 298.15 K and P = 0.1 MPa) for the concentration dependence of the solution chemical potentials of both salt and solvent, their activity coefficients, and the salt solubility, for the recently developed polarizable force fields AH/BK3 of Kiss and Baranyai[37] and AH/SWM4-DP of Lamoureux and Roux.[36] These are compared with experimental results and with previously obtained[27] predictions of the nonpolarizable FF of Joung and Cheatham.[9] We also show predictions and comparisons with experiment of the concentration dependence of the system specific volume, $\overline{v}$, and we examine structural information in terms of pair distribution functions.

In the next section of the paper, we discuss the molecular interaction models studied, followed by a section describing the simulation methodology. The subsequent section describes our results. The final section contains our conclusions and recommendations for future work.

DOI: 10.1021/acs.jctc.5b00018
J. Chem. Theory Comput. 2015, 11, 1756−1764

MOLECULAR MODELS

The AH/SWM4-DP FF employs a four-site water model based on the TIP4P water geometry.[40] The OH bonds and HOH angle are set to their gas phase experimental values, the site charges are $q_M = -2q_H$, and the polarizability is modeled by a charge q_D attached to the oxygen site (which has a counterbalancing charge $-q_D$) by a simple harmonic spring with force constant k_D. The nonpolar interaction between oxygen sites is represented by a Lennard-Jones (LJ) potential with parameters ε and σ. Incorporating an unshielded Coulombic interaction between all intermolecular interaction sites, the complete pair potential between two water molecules assumes the form

$$u_{ij} = u_{\mathrm{LJ},ij} + u_{\mathrm{PC},ij} \tag{1}$$

where

$$u_{\mathrm{LJ},ij} = 4\varepsilon\left[\left(\frac{\sigma}{|\mathbf{r}_{i\mathrm{O}} - \mathbf{r}_{j\mathrm{O}}|}\right)^{12} - \left(\frac{\sigma}{|\mathbf{r}_{i\mathrm{O}} - \mathbf{r}_{j\mathrm{O}}|}\right)^{6}\right] \tag{2}$$

$$u_{\mathrm{PC},ij} = \frac{1}{4\pi\varepsilon_0}\sum_{a,b}\frac{q_{ia}q_{jb}}{|\mathbf{r}_{ia} - \mathbf{r}_{jb}|} \tag{3}$$

and i,j refer to the molecules, a,b refer to the interaction sites of the molecules, and the summation over a,b runs over all five charge sites. The electrolyte is represented by polarizable LJ particles (ions) bearing charge $\pm e$ and immersed in the above water solvent model using Lorentz−Berthelot rules. The polarizability of the ions is also represented by a charge-on-spring model. For further details and the numerical values of all model parameters, see the original papers.[34,36]

The BK3 water FF also assumes the TIP4P water geometry with the gas phase experimental values of the OH bonds and HOH angle but models the nonelectrostatic and electrostatic interactions differently. The oxygen−oxygen interaction is represented by the EXP6 potential

$$u_{\mathrm{EXP6},ij} = \bar{A}\exp(-B|\mathbf{r}_{i\mathrm{O}} - \mathbf{r}_{j\mathrm{O}}|) - C|\mathbf{r}_{i\mathrm{O}} - \mathbf{r}_{j\mathrm{O}}|^{-6} \tag{4}$$

and Gaussian charge distributions are centered on the sites

$$\rho_{ia}(\mathbf{r}) = q_{ia}\exp\left[-\alpha_{ia}^2(\mathbf{r} - \mathbf{r}_{ia})^2\right] \tag{5}$$

where ρ_{ia} is the charge density. The interactions are given by the electrostatic potential energy of two Gaussians

$$u_{\mathrm{GC},ij} = \frac{1}{4\pi\varepsilon_0}\sum_{a,b}\frac{q_{ia}q_{jb}}{|\mathbf{r}_{ia} - \mathbf{r}_{jb}|}\mathrm{erf}(\alpha_{iajb}|\mathbf{r}_{ia} - \mathbf{r}_{jb}|) \tag{6}$$

where

$$\alpha_{iajb} = \frac{\alpha_{ia}\alpha_{jb}}{\sqrt{\alpha_{ia}^2 + \alpha_{jb}^2}} \tag{7}$$

Polarizability is represented (similarly as for SWM4-DP water) by a charge-on-spring model but without introducing additional charged sites: the positions of all three charges are not fixed but attached to each site by springs. The total water−water interaction energy thus assumes a form similar to that of the SWM4-DP potential

$$u_{ij} = u_{\mathrm{EXP6},ij} + u_{\mathrm{GC},ij} \tag{8}$$

but with different forms of the individual site−site potentials. For aqueous NaCl, AH/BK3 models each ion by a polarizable EXP6 interaction with Gaussian distributed charges attached to the particle and Kong combining rules[41] with respect to the EXP6 part of the solvent FF. For further details and parameter values of the model, see the original paper.[37]

As a typical example of a nonpolarizable FF, we considered the Joung−Cheatham (JC) FF,[9] which models the ions as charged Lennard-Jones spheres and Lorentz−Berthelot combining rules, tailored to SPC/E water.[31] The JC parameters are given in the original paper.

COMPUTATIONAL METHODOLOGY

We considered aqueous NaCl solutions at ambient conditions $T = 298.15$ K, $P = 1$ bar. Each liquid simulation was carried out in a cubic simulation box of 270 water particles with periodic boundary conditions and different numbers of ion pairs depending on the concentration. We note in passing that we found that our JC FF results for μ_{NaCl} for the indicated system size agree within simulation uncertainties with those of Mester and Panagiotopoulos,[32] who found negligible finite size effects. On this basis, we believe that our calculations for the other FFs show a similarly negligible system size dependence.

For all liquid simulations, we used the same value of the cutoff radius for the LJ, EXP6, and Coulombic interactions, r_c = 9 Å, and treated the long-ranged Coulombic interactions using the Ewald summation method.[42] Initially, the particles were placed on a face-centered cubic lattice, and rotations of the molecules were generated randomly in the case of liquid systems. For all simulations, we generated configurations using the MPM−MC method.[30,38,39] For the electrolyte chemical potential computations we used the OEMC algorithm, described in detail in our previous papers.[17,23,25] An externally imposed chemical potential serves as an input parameter to determine the corresponding electrolyte concentration.

All chemical potential values are expressed numerically in terms of the same ideal gas reference states as those used in standard thermochemical tables (e.g., the NIST−JANAF Thermochemical Tables[43]). For details concerning numerical values of chemical potentials in our simulations, we refer the reader to an earlier paper.[23]

The molar mean ionic NaCl chemical potential in aqueous solution, μ_{NaCl}, is customarily expressed experimentally in the form of the Henry Law convention on the molality concentration scale

$$\mu_{\mathrm{NaCl}} = \mu_{\mathrm{NaCl}}^{\dagger}(T, P) + 2RT\ln m + 2RT\ln\gamma(T, P, m) \tag{9}$$

where m is the molality in mol kg^{-1} solvent, $\mu_{\mathrm{NaCl}}^{\dagger}(T,P)$ is the molar electrolyte standard state chemical potential at unit molality at the (T,P) of the solution, R is the universal gas constant, and $\gamma(T,P,m)$ is the activity coefficient. (Henceforth, since we consider only ambient conditions, for notational convenience we omit the dependence of quantities on (T, P).) Values of ln γ may be expressed experimentally in the semiempirical form[44]

$$\ln\gamma = \ln(10)\left(-\frac{A\sqrt{m}}{1 + B\sqrt{m}} + bm + cm^2 + dm^3\right) \tag{10}$$

The first term arises from the extended Debye−Hückel theory, and b, c, and d are empirical constants, fitted to data for each electrolyte. A is related to the dielectric permittivity of water for

DOI: 10.1021/acs.jctc.5b00018
J. Chem. Theory Comput. 2015, 11, 1756−1764

Table 2. Parameters in Eqs 9 and 10[a] Obtained by Fitting the (m,μ_{NaCl}) Simulation Data

	$\mu^{\dagger}_{NaCl}$ (kJ mol^{-1})	$\mu^{*}_{H_2O}$ (kJ mol^{-1})	b (kg mol^{-1})	c (kg^2 mol^{-2})	d (kg^3 mol^{-3})
AH/BK3[b]	−398.793	−237.2	0.188599	−0.0290473	0.0017209
AH/BK3[c]	−396.480	−237.2	0.020361	0.0070129	−0.0004715
AH/SWM4-DP[b]	−400.169	−235.2	−0.038951	−0.0115923	0.0012310
JC[d]	−391.278	−240.301	0.019088	0.0215307	−0.0013356
experiment	−393.133[e]	−237.141[f]	0.020442[g]	0.0057927[g]	−0.0002886[g]

[a]For all cases, A = 0.5108, B = 1.4495.[44] [b]($\mu^{\dagger}$,b,c,d) are obtained by fitting the μ_{NaCl} simulation data. [c]$\mu^{\dagger}$ is fixed at the indicated value, and (b,c,d) are obtained by fitting the μ_{NaCl} simulation data. [d]From our previous paper.[26] [e]From Wagman et al.[45] as the sum of the values for Na^+ (−261.905) and Cl^- (−131.228). [f]From the JANAF Thermochemical Tables.[43] [g]From Hamer and Wu.[44]

the FF at the solution (T, P), and B may be treated as an empirical constant. The experimental value of $\mu^{\dagger}_{NaCl}$ is available in thermochemical tables,[45] and values of the constants describing the experimental data for various salt solutions at ambient conditions are available in the compilation of Hamer and Wu.[44] Here, we used their values A = 0.5108 and B = 1.4495 (they used the same value of A for all 1:1 electrolytes and treated B as an empirical constant).

The molar water chemical potential, μ_{H_2O}, can be obtained by integrating the Gibbs−Duhem equation in conjunction with eq 10[26]

$$\mu_{H_2O} = \mu^{*}_{H_2O} - 2RTmM_{H_2O} - RTM_{H_2O}\ln(10) \times \left(bm^2 + \frac{4}{3}cm^3 + \frac{3}{2}dm^4 + \frac{2A}{B^3 + B^4\sqrt{m}} + \frac{4A\ln(B\sqrt{m}+1)}{B^3} - \frac{2A\sqrt{m}}{B^2} - \frac{2A}{B^3} \right) \quad (11)$$

where $\mu^{*}_{H_2O}$ is the chemical potential of pure water at the solution (T,P), and M_{H_2O} is its molecular weight. The experimental value of $\mu^{*}_{H_2O}$ at 298.15 K and 1 bar is −237.141 kJ mol^{-1}.[43]

We expressed our simulation data in the form of eqs 9 and 10 by first performing OEMC simulations at a number of (μ_{NaCl}, m) points and then fitting these equations to the simulation data, treating ($\mu^{\dagger}_{NaCl}$, b, c, d) as fitting parameters (see our previous paper[26] for the details). The experimental values of A and B were used, the precise values of which were found to have only a small effect on the overall quality of the fitted curve (see also the discussion on p 1050 of Hamer and Wu[44]). We then used these parameters to predict μ_{H_2O} using eq 11.

We independently calculated the value of $\mu^{*}_{H_2O}$ using the following variant of the OEMC method. We ran OEMC simulations at the ambient (T, P) for pure water over a range of values of the imposed water chemical potential, μ_{H_2O}. Since the phase rule dictates that two intensive variables determine all others for a pure fluid, the simulation cannot match the imposed μ_{H_2O} value except *exactly* at $\mu^{*}_{H_2O}$; for all other μ_{H_2O} values the simulation exhibits either increasing or decreasing values of the number of water molecules. We determined $\mu^{*}_{H_2O}$ numerically as the midpoint of a small interval of μ_{H_2O} values bounding the change in qualitative behavior of the simulations.

We employed the Frenkel−Ladd thermodynamic integration approach[46,47] to calculate the molar chemical potential of crystalline NaCl, μ_s. The integration comprised 32 steps, gradually changing the interactions of the particles. We calculated the crystal density by standard *NPT* MC simulations. To examine the dependence of the calculated results on system size and to extrapolate to the thermodynamic limit, we considered cases of 256, 500, 864, and 1372 ion pairs, with cutoff radii of (9, 11, 11, 14) Å, respectively, and extrapolated the results to the thermodynamic limit.

We used standard *NPT* MC methodology[42] to calculate the system specific volume as a function of concentration and to examine structural quantities.

RESULTS AND DISCUSSION

We employed the computationally efficient methodology described in the Computational Methodology section to calculate the NaCl molar solid chemical potential and its solubility, in addition to the concentration dependence of the molar chemical potentials of NaCl and of water and the NaCl activity coefficient for aqueous solutions at ambient conditions (T = 298.15 K, P = 0.1 MPa), using the molecular interaction models described in the Molecular Models section. We considered results for the polarizable AH/SWM4-DP force fields of Lamoureux and Roux[36] and of Kiss and Baranyai[35] and compare them with those of the nonpolarizable force field of Joung and Cheatham[9] obtained previously[27] and with experiment. Convenient analytical expressions are given describing the chemical potentials and activity coefficients for each force field considered. We first describe our results for the chemical potential of NaCl in the solution, μ_{NaCl}, and that of its crystalline solid, μ_s, followed by a description of the results for the solubility and for the water chemical potential, μ_{H_2O}. We then describe our results for the activity coefficients. Finally, we show the concentration dependence of the density and display selected structural quantities.

We first calculated several (μ_{NaCl}, m) points spanning a suitable concentration range for each force field using the OEMC algorithm. We then fitted eqs 9 and 10 to the simulation data, fixing the A and B values to those of Hamer and Wu,[44] to obtain the parameters ($\mu^{\dagger}_{NaCl}$, b, c, d), which are listed in Table 2. We found that the fitted μ_{NaCl} curves were insensitive to the precise values of A and B, as was also noted by Hamer and Wu[44] with respect to corresponding fits to experimental data.

The upper panel of Figure 1 shows μ_{NaCl} as a function of concentration for the two polarizable FFs, the nonpolarizable JC FF, and their comparison with the experimental results. The JC μ_{NaCl} values agree slightly better with experiment than those of AH/BK3 at low concentrations, and the reverse is true at higher concentrations. The AH/SWM4-DP values are very low, and they terminate near $m \approx 3$ mol kg^{-1}. A striking aspect of the AH/BK3 curve is its nearly parallel behavior with respect to the experimental curve, deviating from it by an amount of about 3.35 kJ mol^{-1} almost independently of concentration, indicating

DOI: 10.1021/acs.jctc.5b00018
J. Chem. Theory Comput. 2015, 11, 1756−1764

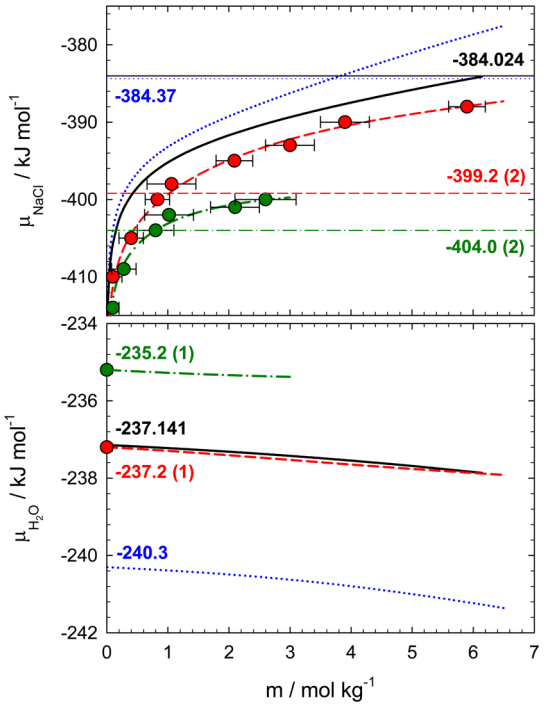

Figure 1. Upper panel: Predicted molar mean ionic electrolyte chemical potential, μ_{NaCl}, of NaCl in aqueous solution at T = 298.15 K and P = 1 bar as a function of molality, m, for the studied force fields, and their comparison with the experimental results. The dashed red curve is the result of eqs 9 and 10 fitted to the simulation data points for the AH/BK3 force field of of Kiss and Baranyai[35] using the indicated parameters in the first row of Table 2; the horizontal red dashed line is the chemical potential of crystalline NaCl for this force field as calculated in this work and given by the indicated value. The dash−dotted green curve is the analogous result for the AH/SWM4-DP force field of Lamoureux and Roux[36] using the parameters in the third row of Table 2, and the dotted blue curve is the analogous result for the force field of Joung and Cheatham[9] using the parameters in the fourth row of Table 2, taken from our previous paper.[26] The solid black curve is the experimental result using the parameters in the last row of Table 2, taken from Hamer and Wu.[44] The horizontal lines indicate the chemical potentials of crystalline NaCl; The AH/BK3 and AH/SWM4-DP results are obtained in this work, the JC result is from our previous paper,[27] and the experimental result is from the NIST−JANAF Thermochemical Tables.[43] The uncertainties of the simulation results (one standard deviation) are indicated. Lower panel: Corresponding predictions for the molar water chemical potential, μ_{H_2O}, as a function of molality. The values near the left axis are those of pure water at T = 298.15 K and P = 1 bar. The AH/BK3[35] and SWM4-DP[36] results were calculated in this work, and the JC results are from our previous paper.[26] The experimental curve is taken from Hamer and Wu,[44] and the chemical potential of pure water is from the NIST−JANAF Thermochemical Tables.[43]

that the slopes of the two curves are very similar; this has important consequences for the μ_{H_2O} and the ln γ curves, as will be explained later in this paper.

The horizontal lines in the upper panel indicate the calculated solid chemical potentials, μ_s, for the different FFs and for the experimental quantity.[43] We performed Frenkel−Ladd calculations as described in the Computational Methodology section in the case of the AH/SWM4-DP and AH/BK3 FFs; the JC result is taken from our previous paper.[26]

The solubility prediction for each FF is given by the intersection of its μ_s value with the corresponding μ_{NaCl} curve. μ_{NaCl} results corresponding to concentrations beyond the respective solubility values represent thermodynamically metastable supersaturated states. Our previous study[27] indicated that these states are computationally stable in the OEMC simulations up to some limiting value of the imposed chemical potential and a corresponding molality, beyond which the simulations diverge. At sufficiently high supersaturation, we found that NPT MC simulations also indicate evidence of nucleation (see, e.g., Figure 5 of the aforementioned paper[27]). We note that similar behavior has been found by Alejandre and Hansen in *NVT* MD simulations.[48] A FF can be expected to provide realistic results at concentrations up to its limiting supersaturation concentration value but not beyond. Although a detailed study of this phenomenon is outside the scope of this paper, we conjecture that the value of the limiting concentration for a given FF is dependent on the simulation ensemble and on the simulation protocols, due in part to different activation energy barriers. The AH/SWM4-DP μ_{NaCl} curve in Figure 1 appears to terminate near m = 3 mol kg^{-1}, a concentration well below the experimental solubility limit of m = 6.144 mol kg^{-1}.[44] The μ_{NaCl} results for the AH/BK3 and JC FFs in Figure 1 are computationally stable and reasonable and extend up to and beyond the experimental solubility value. Since the solid chemical potentials of both polarizable FFs are very low in comparison with the experimental value, their resulting solubility predictions of m = (1.0 ± 0.2) mol kg^{-1} for AH/BK3 and m = (0.8 ± 0.2) mol kg^{-1} for AH/SWM4-DP are also very low. Our recommended value of the JC solubility was reported in our earlier publication[27] and is listed in Table 1. Although its solid chemical potential agrees well with the experimental value, its μ_{NaCl} curve yields a solubility lower than the experimental value.

We calculated $\mu^*_{H_2O}$ for the SWM4-DP and BK3 FFs independently, using the variant of the OEMC method described in the Computational Methodology section. For the JC FF, we used the value from our previous paper,[26] which was obtained by simulating both the electrolyte and water chemical potentials and fitting both sets of results simultaneously to eqs 9−11. The $\mu^*_{H_2O}$ values are listed in Table 2. The lower panel of Figure 1 shows the entire predicted μ_{H_2O} curves for the FFs considered, and the $\mu^*_{H_2O}$ values are indicated on the left axis. The BK3 $\mu^*_{H_2O}$ result is excellent, lying within 0.1 kJ mol^{-1} of the experimental value. In contrast, the SWM4-DP and JC results differ from the experimental value by about +2 kJ mol^{-1} and −3 kJ mol^{-1}, respectively. The disagreement of the JC value with experiment can be attributed in part to its neglect of the polarization energy of the molecules in the liquid, which is unaccounted for in the FF; the AH/SWM4-DP result overestimates this contribution.

The AH/BK3 and AH/SWM4-DP curves for μ_{H_2O} were calculated from eq 11, using the constants obtained by fitting the μ_{NaCl} simulation data. The AH/BK3 curve almost coincides with the experimental curve on the scale of the graph, and the AH/SWM4-DP and JC results are too high and too low, respectively, by amounts similar to the deviations of their predicted values for the pure solvent. The excellent AH/BK3 behavior is a consequence of two factors: (1) the slope of its μ_{NaCl} curve in the upper panel of Figure 1 exhibits good agreement with that of the experimental curve, and (2) its $\mu^*_{H_2O}$ value agrees well with the experimental value. These features

DOI: 10.1021/acs.jctc.5b00018
J. Chem. Theory Comput. 2015, 11, 1756−1764

result in the excellent prediction of μ_{H_2O} from the Gibbs–Duhem equation.

Figure 2 shows the activity coefficient predictions of the force fields studied in terms of ln γ and their comparison with

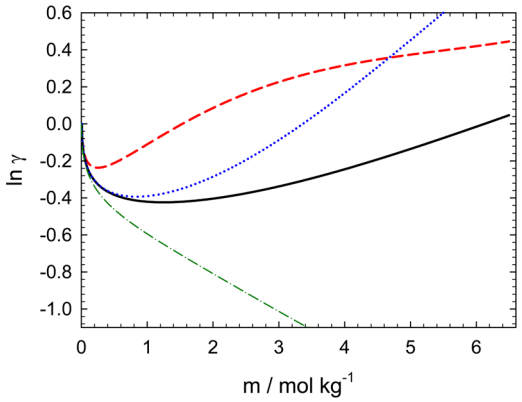

Figure 2. Predicted NaCl activity coefficient, ln γ, of NaCl in aqueous solution at T = 298.15 K and P = 1 bar as a function of the molality, m, for the studied force fields and their comparison with the experimental results. The definitions of the symbols for the curves are given in the caption to Figure 1. The curves are calculated using eqs 9 and 10 fitted to the simulation data, with parameter values in rows 1 and 3–5 of Table 2.

experiment. The curves are determined indirectly, by first fitting eqs 9 and 10 to the μ_{NaCl} simulation data and then using the resulting parameter subset (b, c, d) to calculate ln γ from eq 10. The JC result shows excellent agreement with experiment up to slightly beyond m = 1. For m < 4 it is better than the AH/BK3 result, and for higher concentrations the AH/BK3 result is superior. The AH/SWM4-DP prediction shows the poorest agreement with experiment.

As can be seen from Figure 1 and Table 2, the parameter $\mu^\dagger$ is of similar magnitude to μ_{NaCl}, and the resulting magnitude of ln γ in Figure 2 is much smaller. This indicates that ln γ is very sensitive to the value of $\mu^\dagger$ and that it is best calculated independently and to within an uncertainty of better than about 0.01 kJ mol^{-1}; however, this would require a new simulation methodology and is beyond the scope of the current study. We note that a unique feature of the AH/BK3 ln γ curve in Figure 2 is its roughly constant deviation from and its near parallel course with respect to the experimental curve at moderate and higher concentrations, which is a consequence of the similar behavior of the AH/BK3 μ_{NaCl} shown in Figure 1. We note in passing that the salt activity coefficient derivative is directly related to Kirkwood–Buff integrals,[49] and this curve was previously only obtainable by means of numerical approximations to these integrals at each concentration. This suggests that changing the AH/BK3 $\mu^\dagger$ value by a small amount can potentially improve its agreement of ln γ with the experimental curve, while leaving the fitted μ_{NaCl} curve relatively unchanged. The result of such an exercise is shown in Figure 3. The upper panel shows AH/BK3 ln γ curves calculated using two different parameter sets. The red dashed curve is identical to the one shown in Figure 2, which uses the parameters for eq 10 in the first row of Table 2, obtained by simultaneously fitting the parameter set ($\mu^\dagger$, b, c, d) to the simulated μ_{NaCl} values. The red dotted curve is obtained by fixing $\mu^\dagger$ and then fitting μ_{NaCl} to the reduced parameter set (b, c, d), with the goal of optimizing the agreement with experiment of the ln γ curve of eq 10 with

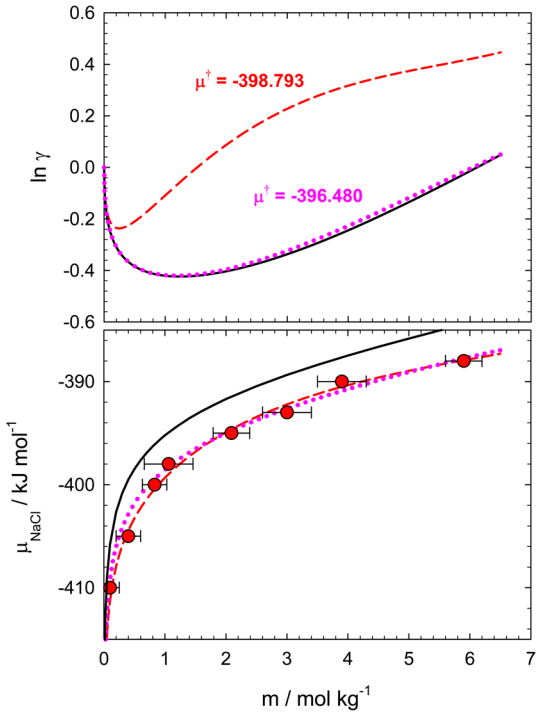

Figure 3. Upper panel: Predicted concentration dependence of the natural logarithm of the NaCl activity coefficient in eqs 9 and 10, ln γ, for the AH/BK3 force field[35] and its comparison with the experimental results. The dashed red curve uses the parameter values in the first row of Table 2, obtained by allowing ($\mu^\dagger$, b, c, d) to be fitting parameters. The dotted red curve uses the parameter values in the second row of Table 2, obtained by fixing $\mu^\dagger$ to the indicated value and fitting the remaining parameters in eqs 9 and 10 to the simulation data. The solid black curve is the experimental result, using eq 10 and parameter values in the last row of Table 2, taken from Hamer and Wu.[44] Lower panel: Corresponding predictions for the concentration dependence of the molar mean ionic electrolyte chemical potential, μ_{NaCl}. The points are the simulation results, and their uncertainties (one standard deviation) are indicated.

respect to the selected value of $\mu^\dagger$. The upper panel of Figure 3 shows that the resulting slightly changed value of $\mu^\dagger$ and its accompanying parameters (b, c, d) in the second row of Table 2 yield essentially perfect agreement of the ln γ curve with experiment. The lower panel shows that the new parameter set results in only minor changes to the μ_{NaCl} curve, which continues to lie within the simulation uncertainties. We note in passing that we found that the ln γ curves for the other FFs in Figure 2 could not be similarly brought into close coincidence with the experimental results by the same approach; the reason is that their differences from the experimental curve show considerable variation with concentration.

The dependence of the specific volume, $\bar{v}$, on molality for the considered FFs is shown in Figure 4, where it is compared with experiment. It is seen that the agreement with experiment of the AH/BK3 predictions is excellent, within the simulation uncertainties up to the experimental solubility. The JC results show a slight underprediction of the experimental results, which increases with increasing concentration. At concentrations below the limiting concentration of $m \lesssim 3$ mol kg^{-1} indicated in the upper panel of Figure 1, the AH/SWM4-DP results also reproduce the experimental data very well, but at higher concentrations they deviate to higher values and show

DOI: 10.1021/acs.jctc.5b00018
J. Chem. Theory Comput. 2015, 11, 1756–1764

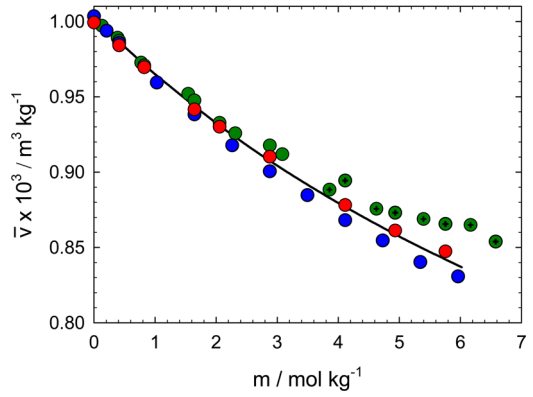

Figure 4. Predicted results for the specific volume, $\bar{v}$ of NaCl in aqueous solution at T = 298.15 K and P = 1 bar as a function of molality, m, using several force fields and their comparison with the experimental results. The orange points indicate the AH/BK3 force field of Kiss and Baranyai,[35] and the green points indicate the AH/SWM4-DP force field of Lamoureux and Roux;[36] the blue points indicate the Joung–Cheatham force field[9] and are taken from our previous paper.[28] The solid curve represents the experimental results, taken from Rogers and Pitzer.[51] The statistical uncertainties of the simulation results lie within the size of the symbols.

considerable scatter, possibly indicating the onset of nucleation of the salt, indicated in the upper panel of Figure 1.

Finally, Figure 5 shows representative pair distribution functions for the two polarizable FFs at m = 2.878 mol kg^{-1},

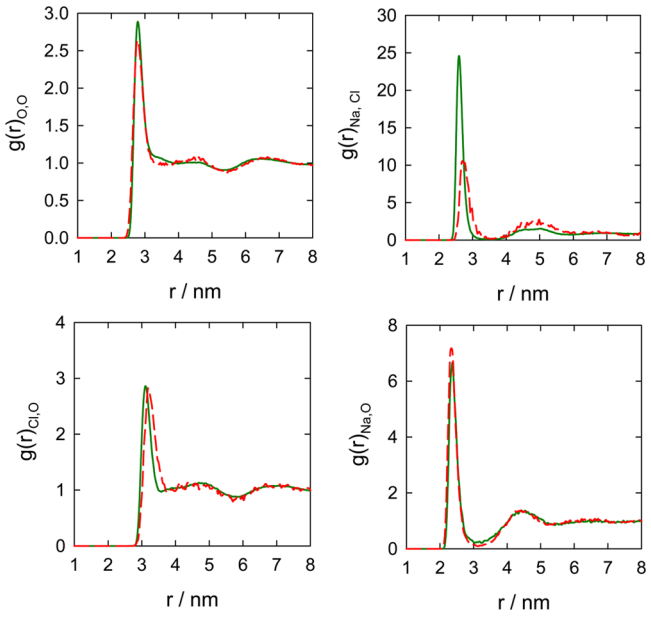

Figure 5. Radial distribution functions using several force fields for an aqueous NaCl solution at T = 298.15 K and P = 1 bar and molality m = 2.878 mol kg^{-1}. The dashed red curve is obtained using the AH/BK3 force field of Kiss and Baranyai,[35] and the solid green curve is obtained using the AH/SWM4-DP force field of Lamoureux and Roux.[36]

which is slightly below the apparent AH/SWM4-DP limiting concentration shown in Figure 1. The O–O and ion–O $g(r)$ curves are similar, indicating that the water–ion portions of the FFs are somewhat similar. However, the ion–ion $g(r)$ curves are quite different, particularly for the first peak, with the AH/SWM4-DP result indicating much stronger ion pairing than for the AH/BK3 case. This behavior is consistent with the relatively lower AH/BK3 solid chemical potential shown in Figure 1 and may be a precursor to the onset of homogeneous nucleation above its limiting concentration near m = 3 mol kg^{-1}.

CONCLUSIONS

The calculation of aqueous electrolyte chemical potentials over a broad concentration range is an important and computationally challenging problem that has not been extensively studied in the literature, and these challenges are magnified when polarizable force fields are used. In this paper, we have demonstrated the use of a computationally efficient algorithm for such calculations that combines the Osmotic Ensemble Monte Carlo algorithm[17,23,25−28] with the Multiple Particle Move Monte Carlo method.[30,38,39] We have used this approach to compute the predictions at ambient conditions for aqueous NaCl solutions of the polarizable AH/BK3 FF of Kiss and Baranyai[37] and the AH/SWM4-DP FF of Lamoureux and Roux[36] for the concentration dependence of the electrolyte and solvent chemical potentials and for the electrolyte activity coefficient, in addition to the solid chemical potential and the solubility. We calculated the chemical potential of pure water at ambient conditions for each polarizable FF using a variant of the OEMC methodology. We have also calculated the concentration dependence of the solution specific volume and compared all results with those of the nonpolarizable FF of Joung and Cheatham[9] compatible with SPC/E water (JC) and with the experimental quantities.

Electrolyte Chemical Potential, μ_{NaCl}:

1. The AH/BK3 μ_{NaCl} is in reasonable agreement with experiment, differing from it by an almost concentration-independent value of about 3.35 kJ mol^{-1} at moderate and higher concentrations, i.e., the curves have very similar derivatives. This results in an excellent prediction of the water chemical potential with respect to experiment and an activity coefficient that is also nearly parallel to the experimental result (see further discussion below).

2. The AH/SWM4-DP μ_{NaCl} curve shows generally poor agreement with experiment. In our simulations, the curve appears to exhibit a limiting concentration at $m \approx 3$ mol kg^{-1}, beyond which there is evidence of homogeneous nucleation in the OEMC simulations, slow convergence of the specific volume in *NPT* simulations, and the resulting specific volume values differ significantly from the experimental data. Slightly below its limiting concentration, AH/SWM4-DP predicts significantly stronger ion pairing than does AH/BK3, possibly indicating this behavior is a precursor to homogeneous nucleation.

3. The JC μ_{NaCl} agrees somewhat better with experiment than does that of AH/BK3 at low concentrations, but this is reversed at moderate and higher concentrations.

Electrolyte Activity Coefficient:

1. The electrolyte activity coefficient in the Henry law molality model of eq 9 calculated from the total electrolyte chemical potential is very sensitive to the value used for the standard state chemical potential $\mu^{\dagger}$. However, since the AH/BK3 activity coefficient derivative curve is nearly parallel to the experimental curve at moderate and higher concentrations, the AH/BK3 ln γ curve can be brought into excellent agreement with experiment by an appropriate value of $\mu^{\dagger}$. This curve has only previously been available for a given force field by an

DOI: 10.1021/acs.jctc.5b00018
J. Chem. Theory Comput. 2015, 11, 1756−1764

approximate numerical integration of Kirkwood−Buff integrals at each concentration.

2. The AH/SWM4-DP activity coefficients show poor agreement with experiment.

3. The JC activity coefficient predictions deviate increasingly from the experimental values beyond $m \approx 1$.

Water Chemical Potential, μ_{H_2O}:

1. The BK3 value of the chemical potential of pure water at ambient conditions, $\mu^*_{H_2O} = -237.2 \pm 0.1$ kJ mol^{-1}, is in excellent agreement with the experimental value[43] of −237.1 kJ mol^{-1}. The combination of this fact with item 1 for μ_{NaCl} above causes the AH/BK3 μ_{H_2O} predicted from μ_{NaCl} and the Gibbs−Duhem equation to agree very well with the experimental results over the entire experimentally accessible concentration range.

2. The AH/SWM4-DP $\mu^*_{H_2O}$ value of −235.2 ± 0.1 kJ mol^{-1} is too high in comparison with experiment, which results in its predicted μ_{H_2O} curve being much higher than the experimental result.

3. The JC $\mu^*_{H_2O}$ value of −240.3 kJ mol^{-1} is too low, which results in its predicted μ_{NaCl} curve being much lower than the experimental result.

Solid Chemical Potential and Solubility:

1. The AH/BK3 and AH/SWM4-DP solid chemical potential predictions lie well below the experimental value[43] of −384.024 kJ mol^{-1} (−399.0 ± 0.2 kJ and −403.8 ± 0.2, respectively). Both force fields predict very low solubility values (1.0 ± 0.2 mol kg^{-1} for AH/BK3 and 0.8 ± 0.2 mol kg^{-1} for AH/SWM4-DP) in comparison with the experimental value[44] of 6.144 mol kg^{-1}.

2. The solid chemical potential prediction of the JC FF[27] (−384.37 kJ mol^{-1}) is in excellent agreement with experiment, but its too high chemical potential curve with respect to experiment results in a solubility of 3.64(20) mol kg^{-1} that is too low.[27]

Specific Volume:

1. The concentration dependence of the predicted AH/BK3 specific volume is in excellent agreement with that of experiment.

2. The AH/SWM4-DP specific volume is in good agreement with experiment at molalities below its limiting concentration of $m \approx 3$. At higher concentrations it deviates to higher values and shows considerable scatter, possibly indicating the onset of nucleation of the salt at concentrations above the limiting concentration.

3. The JC specific volume is of only slightly lower quality than the AH/BK3 predictions.

AUTHOR INFORMATION

Corresponding Author

*E-mail: william.smith@uoit.ca.

Notes

The authors declare no competing financial interest.

ACKNOWLEDGMENTS

Support for this work was provided by the Natural Sciences and Engineering Research Council of Canada (Discovery Grant OGP1041), the SHARCNET (Shared Hierarchical Academic Research Computing Network) HPC consortium (http://www.sharcnet.ca), the Czech National Science Foundation (Grant No. GP13-35793P), and the Czech Ministry of Education, Youth and Sport (Project No. LH12019).

REFERENCES

(1) Theodoru, D. N. Progress and outlook in Monte Carlo simulations. *Ind. Eng. Chem. Res.* **2010**, *49*, 3047−3058.

(2) Auffinger, P.; Cheatham, T. E., III; Vaiana, A. C. Spontaneous formation of KCl aggregates in biomolecular simulations: A force field issue? *J. Chem. Theory Comput.* **2007**, 1851−1858.

(3) Ungerer, P.; Nieto-Draghi, C.; Rousseau, B.; Ahunbay, G.; Lachet, V. Molecular simulation of the thermophysical properties of fluids: From understanding toward quantitative predictions. *Mol. Simul.* **2010**, *134*, 71−89.

(4) Chen, A. A.; Pappu, R. V. Parameters of monovalent ions in the AMBER-99 forcefield: Assessment of inaccuracies and proposed improvements. *J. Phys. Chem. B* **2007**, *111*, 11884−11887.

(5) Maginn, E. J.; Elliott, J. R. Historical perspective and current outlook for Molecular Dynamics as a chemical engineering tool. *Ind. Eng. Chem. Res.* **2010**, *49*, 3059−3078.

(6) Meunier, M. *Industrial Applications of Molecular Simulations*; CRC Press: Boca Raton, FL, 2011.

(7) Dror, R. O.; Dirks, R. M.; Grossman, J. P.; Xu, H.; Shaw, D. E. Biomolecular simulation: A computational microscope for molecular biology. *Annu. Rev. Biophys.* **2012**, *41*, 429−452.

(8) Aqvist, J. Ion-water interaction potentials derived from free energy perturbation simulations. *J. Phys. Chem.* **1990**, *94*, 8021−8024.

(9) Joung, I. S.; Cheatham, T. E., III Determination of alkali and halide monovalent ion parameters for use in explicity solvated biomolecular simulations. *J. Phys. Chem. B* **2008**, *112*, 9020−9041.

(10) Luo, Y.; Roux, B. Simulation of osmotic pressure in concentrated aqueous salt solutions. *J. Phys. Chem. Lett.* **2010**, *1*, 183−189.

(11) Mazur, A. K. Titration in silico of reversible B**A transitions in DNA. *J. Am. Chem. Soc.* **2003**, *125*, 7849−7859.

(12) Cheatham, T. E., III Simulations and modeling of nucleic acid structure, dynamics and interactions. *Curr. Opin. Struct. Biol.* **2004**, *14*, 360−367.

(13) Savelyev, A.; Papoian, G. A. Electrostatic, steric, and hydration interactions favor Na(+) condensation around DNA compared with K(+). *J. Am. Chem. Soc.* **2006**, *128*, 14506−14518.

(14) Savelyev, A.; Papoian, G. A. Inter-DNA electrostatics from explicit solvent molecular dynamics simulations. *J. Am. Chem. Soc.* **2006**, *129*, 6060−6061.

(15) Yang, Y.; Meng, S. Atomistic nature of NaCl nucleation at the solid-liquid interface. *J. Chem. Phys.* **2007**, *126*, 044708.

(16) Mocci, F.; Laaksonen, A. Insight into nucleic acid counterion interactions from inside molecular dynamics simulations is "worth its salt". *Soft Matter* **2012**, *8*, 9268−9284.

(17) Lísal, M.; Smith, W. R.; Kolafa, J. Molecular simulations of aqueous electrolyte solubility: 1. The expanded-ensemble osmotic molecular dynamics method for the solution phase. *J. Phys. Chem. B* **2005**, *109*, 12956−12965.

(18) Sanz, E.; Vega, C. Solubility of KF and NaCl in water by molecular simulation. *J. Chem. Phys.* **2007**, *126*, 014507.

(19) Joung, I. S.; Cheatham, T. E., III Molecular dynamics simulations of the dynamic and energetic properties of alkali and halide ions using water-model-specific ion parameters. *J. Phys. Chem. B* **2009**, *113*, 13279−13290.

(20) Paluch, A. S.; Jayaraman, S.; Shah, J. K.; Maginn, E. J. A method for computing the solubility limit of solids: Application to sodium chloride in water and alcohols. *J. Chem. Phys.* **2010**, *133*, 124504.

(21) Paluch, A. S.; Jayaraman, S.; Shah, J. K.; Maginn, E. J. Erratum: "A method for computing the solubility limit of solids: Application to sodium chloride in water and alcohols". *J. Chem. Phys.* **2010**, *133*, 124504; *J. Chem. Phys.* **2012**, *137*, 039901.

(22) Zhang, C.; Raugei, S.; Eisenberg, R.; Carloni, O. Molecular dynamics in physiological solutions: Force fields, alkali metal ions and ionic strength. *J. Chem. Theory Comput.* **2010**, *6*, 2167−2175.

DOI: 10.1021/acs.jctc.5b00018
J. Chem. Theory Comput. 2015, 11, 1756−1764

(23) Moučka, F.; Lísal, M.; Škvor, J.; Jirsák, J.; Nezbeda, I.; Smith, W. R. Molecular simulation of aqueous electrolyte solubility. 2. Osmotic ensemble Monte Carlo methodology for free energy and solubility calculations and application to NaCl. *J. Phys. Chem. B* **2011**, *115*, 7849−7861.
(24) Aragones, J. L.; Sanz, E.; Vega, C. Solubility of NaCl in water by molecular simulation revisited. *J. Chem. Phys.* **2012**, *136*, 244508.
(25) Moučka, F.; Lísal, M.; Smith, W. R. Molecular simulation of aqueous electrolyte solubility. 3. Alkali-halide salts and their mixtures in water and in hydrochloric acid. *J. Phys. Chem. B* **2012**, *116*, 5468−5478.
(26) Moučka, F.; Nezbeda, I.; Smith, W. R. Molecular simulation of aqueous electrolytes: Water chemical potential results and Gibbs-Duhem equation consistency tests. *J. Chem. Phys.* **2013**, *139*, 124505.
(27) Moučka, F.; Nezbeda, I.; Smith, W. R. Molecular force fields for aqueous electrolytes: SPC/E-compatible charged LJ sphere models and their limitations. *J. Chem. Phys.* **2013**, *138*, 154102.
(28) Moučka, F.; Nezbeda, I.; Smith, W. R. Molecular force field development for aqueous electrolytes: 1. Incorporating appropriate experimental data and the inadequacy of simple electrolyte force fields based on Lennard-Jones and point charge interactions with Lorentz-Berthelot rules. *J. Chem. Theory Comput.* **2013**, *9*, 5076−5085.
(29) Kobayashi, K.; Liang, Y.; Sakka, T.; Matsuoka, T. Molecular dynamics study of salt-solution interface: Solubility and surface charge of salt in water. *J. Chem. Phys.* **2014**, *140*, 144705.
(30) Moučka, F.; Nezbeda, I.; Smith, W. R. Computationally efficient Monte Carlo simulations for polarisable models: multi-particle move method for water and aqueous electrolytes. *Mol. Simul.* **2013**, *39*, 1125−1134.
(31) Berendsen, H. J. C.; Grigera, J. R.; Straatsma, T. P. The missing term in effective pair potentials. *J. Phys. Chem.* **1987**, *91*, 6269−6271.
(32) Mester, Z.; Panagiotopoulos, A. Z. Mean ionic activity coefficients in aqueous NaCl solutions from molecular dynamics simulations. *J. Chem. Phys.* **2015**, *142*, 044507.
(33) Guillot, B. A reappraisal of what we have learnt during three decades of computer simulations on water. *J. Mol. Liq.* **2002**, *101*, 219−260.
(34) Lamoureux, G.; MacKerell, A. D.; Roux, B. A simple polarizable model of water based on classical Drude oscillators. *J. Chem. Phys.* **2003**, *119*, 5185−5197.
(35) Kiss, P. T.; Baranyai, A. A systematic development of a polarizable potential of water. *J. Chem. Phys.* **2013**, *138*, 204507.
(36) Lamoureux, G.; Roux, B. Absolute hydration free energy scale for alkali and halide ions established from simulations with a polarizable force field. *J. Phys. Chem. B* **2006**, *110*, 3308−3322.
(37) Kiss, P. T.; Baranyai, A. A new polarizable force field for alkali and halide ions. *J. Chem. Phys.* **2014**, *141*, 114501.
(38) Moučka, F.; Rouha, M.; Nezbeda, I. Efficient multiparticle sampling in Monte Carlo simulations on fluids: Application to polarizable models. *J. Chem. Phys.* **2007**, *126*, 224106.
(39) Moučka, F.; Nezbeda, I. The multi-particle sampling method in Monte Carlo simulations on fluids and its efficient implementations. *Mol. Simul.* **2010**, *36*, 526−534.
(40) Jorgensen, W. L.; Chandrasekhar, J.; Madura, J. D.; Impey, R. W.; Klein, M. L. Comparison of simple potential functions for simulating liquid water. *J. Chem. Phys.* **1983**, *79*, 926−935.
(41) Kong, C. L.; Chakrabarty, M. R. Combining rules for intermolecular potential parameters. III. Application to the exp 6 potential. *J. Phys. Chem.* **1973**, *77*, 2668−2670.
(42) Allen, M. P.; Tildesley, D. J. *Computer Simulation of Liquids*; Oxford University Press: Oxford, 1987.
(43) Chase, M. W., Jr. *NIST-JANAF Thermochemical Tables, J. Phys. Chem. Ref. Data, Monograph No. 9*; Am. Chem. Soc. and Am. Inst. of Physics: Woodbury, NY, 1998.
(44) Hamer, W. J.; Wu, Y.-C. Osmotic coefficients and mean activity coefficients of univalent electrolytes in water at 25 °C. *J. Phys. Chem. Ref. Data* **1972**, *1*, 1047−1099.
(45) Wagman, D. D.; Evans, W. H.; Parker, V. B.; Schumm, R. H.; Halow, I.; Bailey, S. M.; Churney, K. L.; Nuttall, R. L. The NBS tables of chemical thermodynamic properties: Selected values for inorganic and C_1 and C_2 organic substances in SI units. *J. Phys. Chem. Ref. Data* **1982**, Vol. *11*, Suppl. 2.
(46) Frenkel, D.; Ladd, A. J. C. New Monte Carlo method to compute the free energy of arbitrary solids. Application to the fcc and hcp phases of hard spheres. *J. Chem. Phys.* **1984**, *81*, 3188−3193.
(47) Anwar, J.; Frenkel, D.; Noro, M. G. Calculation of the melting point of NaCl by molecular simulation. *J. Chem. Phys.* **2003**, *118*, 728−735.
(48) Alejandre, J.; Hansen, J.-P. Ions in water: From ion clustering to crystal nucleation. *Phys. Rev. E* **2007**, *76*, 061505.
(49) Gee, M. B.; Cox, N. R.; Jiao, Y.; Bentenitis, N.; Weerasinghe, S.; Smith, P. E. A Kirkwood-Buff derived force field for aqueous alkali halides. *J. Chem. Theory Comput.* **2011**, *7*, 1369−1380.
(50) Smith, D. E.; Dang, L. X. Computer simulations of NaCl association in polarizable water. *J. Chem. Phys.* **1994**, *100*, 3757−3766.
(51) Rogers, P. S. Z.; Pitzer, K. S. J. Volumetric properties of aqueous sodium chloride solutions. *J. Phys. Chem. Ref. Data* **1982**, *11*, 15−81.

DOI: 10.1021/acs.jctc.5b00018
J. Chem. Theory Comput. 2015, 11, 1756−1764